Available online at www.sciencedirect.com
ScienceDirect
Journal of the European Ceramic Society 27 (2007) 367–376
www.elsevier.com/locate/jeurceramsoc

Microstructural characterization using orientation imaging microscopy of cellular Si/SiC ceramics synthesized by replication of Indian dicotyledonous plants

V. Pancholi [a], D. Mallick [b], Ch. AppaRao [c], I. Samajdar [a], O.P. Chakrabarti [b,*], H.S. Maiti [b], R. Majumdar [d]

[a] *Department of Metallurgical Engineering and Materials Science, Indian Institute of Technology, Bombay, Powai, Mumbai 400076, India*
[b] *Central Glass and Ceramic Research Institute, 196 Raja S.C. Mullick Road, Kolkata 700032, India*
[c] *Department of Metallurgical Engineering, JNTU College of Engineering, Jawaharlal Nehru Technological University, Hyderabad 500072, India*
[d] *Department of Chemical Technology, University of Calcutta, 92 A.P.C Road, Kolkata 700009, India*

Received 10 September 2005; received in revised form 28 April 2006; accepted 6 May 2006
Available online 21 June 2006

Abstract

Woods from three dicotyledonous plants of local origin (mango *Mangifera indica*), jackfruit (*Artocarpus integrifolia*) and teak (*Tectona grandis*) were transformed by pyrolysis into carbonaceous preforms and subsequently converted into cellular Si/SiC ceramics by liquid Si-infiltration and reaction. The pyrolyzed mango, jackfruit and teak were characterized in terms of pyrolysis weight loss, shrinkages, bulk density and microstructures. The Si-infiltrated pyrolyzed woods were found to have densities and porosities in the range of 2.46–2.60 gm cm^{-3} and 1.5–3.6 vol.% respectively. SEM imaging confirmed the preservation of microcellular tissue anatomy of the precursor wood structure in the morphologies of final ceramics. The end ceramics were investigated for the phases present and for crystallographic microtexture. A combination of XPS (X-ray photoelectron spectroscopy), XRD (X-ray diffraction) and OIM (orientation imaging microscopy) was used to establish the presence and the relative locations of silicon (Si), silicon carbide (SiC) and graphite (C). Fine SiC grains did typically surround coarse crystals of Si – the latter had significant presence of Σ3 twin boundaries. Graphite was primarily present in the regions containing SiC and was more textured than the SiC. Distinct orientation relationship could be established between the graphite crystals and the Si grains containing them.

Keyword: Cellular ceramics; Si/SiC; SiC; Biomorphic materials

1. Introduction

In recent years much attention has been focused on the synthesis of engineering ceramics and composites in the image of biostructures.[1–5] Plants often possess natural composite structures and it has been possible to produce novel SiC based materials by replicating hierarchically designed composite morphology of plant structures. Duplex Si/SiC ceramic composite, an industrially important engineering material, which is conventionally prepared by liquid silicon infiltration (LSI) technique[6,7] involving expensive synthetic raw material powders of desirable quality and complex green shape making, can also be prepared following transformation of bioorganic structures, especially plant structures inherent in wood and stem into ceramic structures. A number of recent publications and patents[8–18] has dealt with different aspects of such processing. The most common practice is to make use of some wood or other plant material, suitably pieced and/or shaped, in the preparation of a carbonized preform under controlled condition of thermal processing and allow the latter to react with silicon bearing liquid or gas under vacuum or in an inert atmosphere. The cellular SiC based ceramics are property-wise comparable to their conventional counterparts.[9,10,18] It has been pointed out that caudex stems of monocotyledons are structurally different from dicotyledonous woods and that replication of these structures in SiC ceramics can lead to microstructurally different materials.[16,17] Recent communications deal with the preliminary aspects of the processing and characterization of cellular

* Corresponding author. Tel.: +91 33 2473 3496; fax: +91 33 2473 0957.
E-mail address: omprakash@cgcri.res.in (O.P. Chakrabarti).

0955-2219/$ – see front matter © 2006 Elsevier Ltd. All rights reserved.
doi:10.1016/j.jeurceramsoc.2006.05.083

Table 1
Characteristics of native dicotyledonous woods used in the present study

Characteristics	Wood		
	Jackfruit	Mango	Teak
1. Molecular composition (wt.%)			
(i) α-Cellulose[a]	38.05	37.60	35.92
(ii) Hemicellulose[a]	25.00	26.64	21.35
(iii) Lignin[a]	33.10	31.80	39.45
(iv) Ash[a]	0.48	1.29	0.77
(v) Moisture[a]	11.03	11.68	9.78
2. Density(g cm^{-3})	0.58 ± 0.03	0.57 ± 0.01	0.64 ± 0.01
3. Drying loss (%)	10.41	9.93	10.16
4. Drying shrinkage (%)			
Axial	0.14	0.13	0.08
Radial	1.92	1.96	0.97
Tangential	4.55	3.36	0.98

[a] For details of the test procedure, see Ref. [19].

Si/SiC ceramics derived by replicating the structure of some Indian dicotyledonous woods[19] and attempt at a comparison of dicot wood and monocot stem as plant precursors for synthesis of Si/SiC based engineering ceramics.[20] Characterization of cellular SiC based ceramics normally involves different microscopic techniques.[9,18,19,21–25] An emerging technique of orientation imaging microscopy (OIM) has been used in a limited way.[9]

A relatively fast acquisition and automated indexing of backscattered Kikuchi diffraction has made OIM a promising technique for microstructural characterization.[26] The technique provides information not only on microstructure, but also on the microtexture – the orientations of grains and phases present. There are two limitations, especially relevant to the present study, – (i) the spatial resolution of OIM is typically of the order of 0.5 μm and (ii) the technique cannot distinguish between phases with identical crystal structures. The present study was formulated to exploit the potentials of OIM characterization in understanding the microtextural developments in cellular Si/SiC ceramics synthesized from common Indian dicotyledonous trees with preservation of morphological and structural characteristics of the precursor plants.

2. Experimental

2.1. Material synthesis

2.1.1. Pyrolytic conversion of plant materials into carbonaceous performs

Woods of three common dicotyledonous plants of local origin (mango (*Mangifera indica*), jackfruit (*Artocarpus integrifolia*) and teak (*Tectona grandis*)) were used as precursors, the characteristics of which are given in Table 1. Wood specimen was shaped, dried and pyrolyzed by heating up to 800 °C in an electrically heated furnace to yield rectangular biocarbon perform (70 mm × 13 mm × 13 mm), the procedural details have been described elsewhere.[19] It was further characterized in terms of pyrolytic weight loss, shrinkage, bulk density and microstructure.

2.1.2. Ceramization of carbon perform

The biocarbon preforms were infiltrated and reacted with molten silicon at around 1600 °C to yield duplex Si/SiC ceramic and the end material was characterized in terms of density, porosity, presence of crystalline phases, microstructure and oxidation resistance (1350 °C), as reported earlier.[19]

2.2. X-ray measurements

XRD was carried out on a Panalytical MRD system, using Co Kα source. X-ray photoelectron spectroscopy (XPS) was performed using a Multilab Thermo VG Scientific CLAM-4 instrument with an Mg Kα X-ray excitation source ($h\nu$ = 1253.6 eV); binding energies (B.E.) were determined with respect to the position of the Au $4f_{7/2}$ peak at 83.9 eV. The survey spectra, collected over a range of 0–1100 eV, and high-resolution spectra were acquired using a pass-energy of 50 eV. The residual pressure in the analysis chamber was maintained below 10^{-9} Torr during data acquisition.

2.3. Microtexture measurements

2.3.1. Electron backscattered diffraction (EBSD) technique

EBSD is an ideal technique to determine the microtexture of the phases present in a system. The technique utilizes the generation of Kikuchi pattern due to diffraction of scattered electrons satisfying the Bragg's condition from the lattice planes. The Kikuchi pattern consists of bands (two parallel lines), where each band corresponds to a crystallographic plane. The quality of the acquired diffraction pattern is indicated by the image quality (IQ). The quality of Kikuchi pattern depends (indexed in EBSD as IQ – the IQ parameter is the sum of the detected peaks in the Hough transform) on strain (relative inelastic scattering resulting from defects) and on phases present (phase with higher atomic number give stronger pattern).

2.3.2. Sample preparation

The samples for local orientation measurement were prepared using standard polishing technique. To remove the damaged layer introduced during polishing process, final polishing was carried out using 0.5 μm colloidal silica and a suitable etch polish cycle. A TSL (Tex-Sem laboratories) OIM (orientation imaging microscopy) system on a FEI quanta 200 HV microscope was used for the measurements. Multiple scans were done, covering total area of at least 1000 μm × 1200 μm on each sample using step size of 0.5 μm.

3. Results

3.1. Material synthesis

3.1.1. Pyrolytic conversion of woods to skeletal carbon preform

During pyrolysis runs all the three wood samples exhibited weight losses to the extent of 67–69% of dry mass. Mango, jackfruit and teak all had similar pyrolytic axial shrinkages of around 22%. They differed widely in radial and tangential shrinkages.

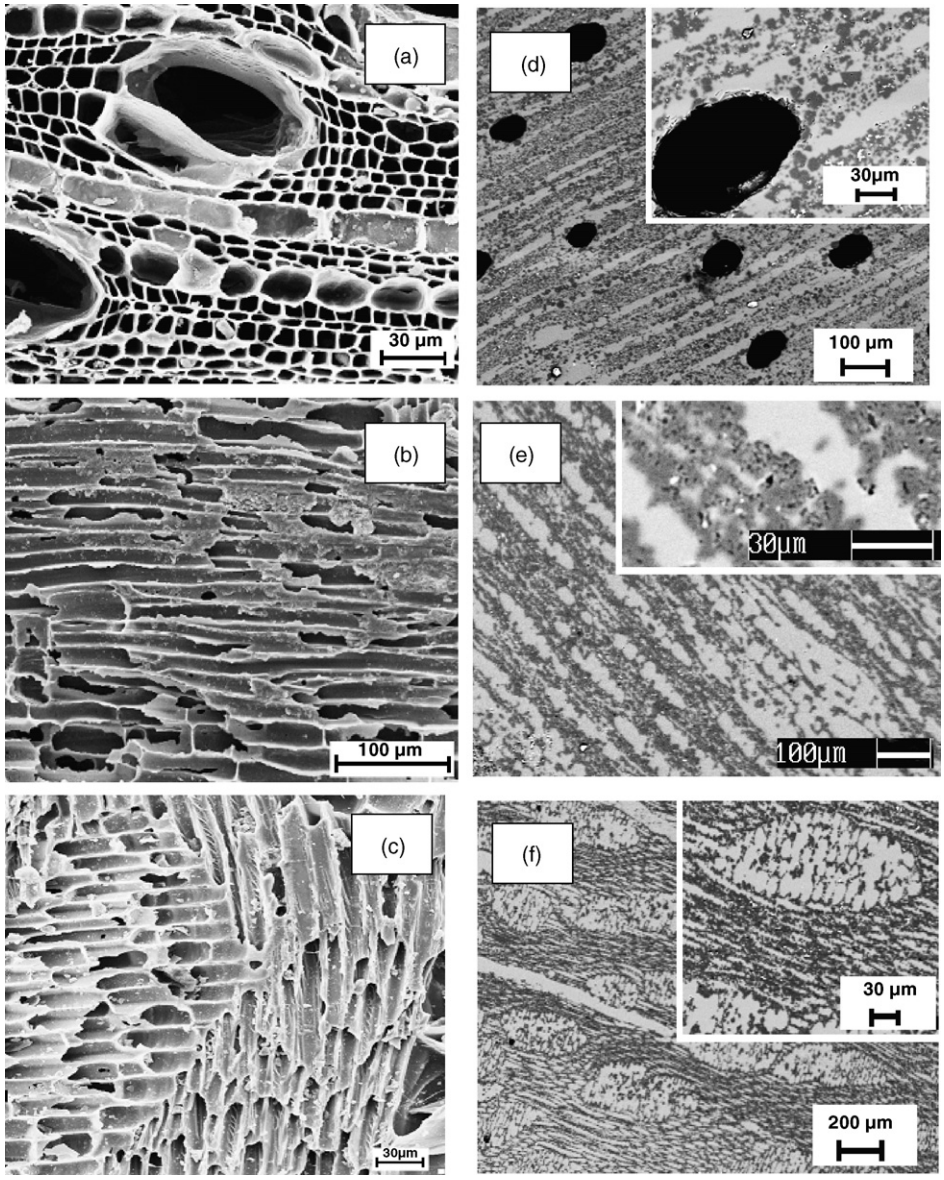

Fig. 1. Replication of cellular structural features of Indian dicot woods in ceramics – SEM/SE images of (a) tangential–radial (TR) and (b) axial–radial (AR) sections of pyrolyzed mango and (c) AR section of pyrolyzed teak; SEM/BSE images of (d) TR- and (e) AR sections of Si/SiC – mango and (f) AR section of Si/SiC – teak.

While mango and jackfruit exhibited high, up to around 26–27% shrinkage in radial direction, the same for teak had been recorded to be around 12%. In case of tangential pyrolytic shrinkage the difference was remarkable – around 30–33%, 13–15% and 6–7% shrinkages were observed for pyrolyzed mango, jackfruit and teak respectively. The density values of the biocarbon preforms derived from mango, jackfruit and teak were measured to be 0.39, 0.33 and 0.29 gm cm^{-3} respectively. It had been observed that microstructural features in biocarbon preforms from dicot woods were highly anisotropic and change in different directions with respect to the growth axis of the native plant.[19,20] Fig. 1(a)–(c) typically represent the microstructural views of tangential–radial (TR) and axial–radial (AR) sections of biocarbon preform from mango and also axial–radial (AR) section of pyrolyzed teak woods respectively, showing characteristic arrangement of carbon web along with porous channels originating from vascular vessels and tracheidal cells present in the precursor plants.

3.1.2. Ceramization of carbon preform

Spontaneous infiltration of the biocarbon preforms took place when the tracheidal pore system was brought into contact with the silicon melt. All the specimens got fully infiltrated and reacted throughout into dense structures with complete retention of the macroscopical structural integrity. The Si-infiltrated pyrolyzed mango showed the highest density of 2.60 gm cm^{-3} at the porosity level of 1.5 vol.%. The density and porosity values for Si/SiC – jackfruit and teak were 2.53 and 2.46 gm cm^{-3} and 2.5 and 3.6 vol.%, respectively. The infiltrated density followed the order of density obtained with biocarbon preforms derived from different wood specimens. The XRD-scans of the bulk specimen of Si infiltrated pyrolyzed woods were similar

showing the presence of β-SiC and Si as the only crystalline phases. The appearance of dense microstructure was common in both the tangential–radial (TR) and the axial–radial (AR) sections.[19] SEM examination of the Si melt infiltrated pyrolyzed wood samples showed that the microstructural features of the initial native preform were well preserved during transformation into ceramic structures. Fig. 1(d)–(f) typically represent the SEM/BSE images of tangential–radial (TR) and axial–radial (AR) sections of Si-infiltrated pyrolyzed mango and axial–radial (AR) section of Si-infiltrated pyrolyzed teak respectively. Three phases are observed viz., predominant dark grey regions, light grey zones and occasional deep black spots; the first two phases were detected as SiC and Si respectively by EDX analysis and the deep black spots were identified as pores and/or residual carbon. The pyrolyzed woods originally contained porous channels arising out of the tracheidal vessels present in the precursor plants and such pores are seen to be nearly completely filled with solidified Si with the carbon of the pyrolyzed preform converting primarily to β-SiC after processing. In the infiltrated specimens large pores (Fig. 1(d)), originating from the vascular channels, that remain unfilled with Si, are also seen. The residual carbon still present after processing, is mainly due to local density variations in the carbon preform. Especially in more dense areas, the carbon density exceeded the critical limit of about 0.97 g/cm^3 clogging the pores during Si infiltration and inhibiting further SiC-formation.[27]

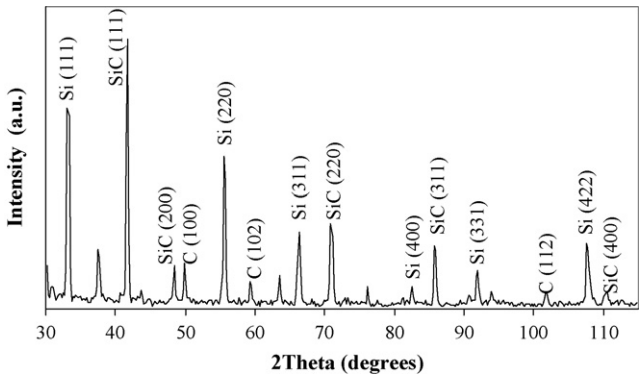

Fig. 2. XRD spectra of the Si/SiC – jackfruit. Peaks of Si, SiC and graphite (C) are marked adjacent to the observed peak. Intensity is in arbitrary unit (a.u.).

3.2. XRD measurement

Preliminary identification of phases present in the composite was obtained using XRD – see Fig. 2, a typical XRD of the

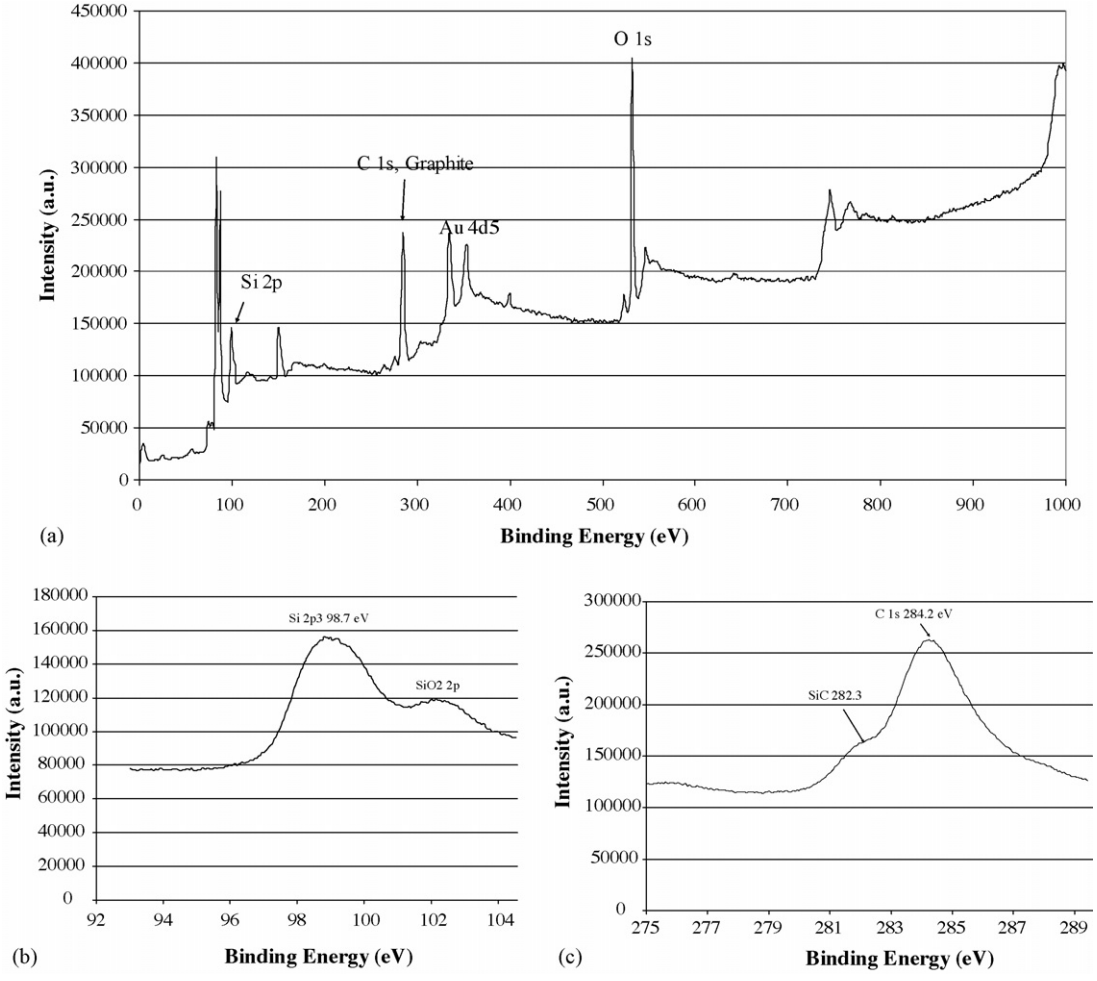

Fig. 3. The XPS spectra of Si/SiC composite (a) survey spectrum, (b) high resolution spectrum of Si 2p and (c) high resolution spectrum of C 1s.

composite synthesized from jackfruit wood. Similar results were obtained in the other two types of composites as well. XRD could establish presence of cubic Si and SiC (β-SiC) and hexagonal graphite phases.

3.3. XPS

XPS is not an imaging technique and interpretations in inhomogeneous system(s) are difficult. XPS results support and complement the XRD results. Fig. 3 shows the acquired XPS spectra of Si 2p (Fig. 3(b)) and C 1s (Fig. 3(c)) respectively. The peak occurring at 98.7 eV was attributed to Si–Si bond (Fig. 3(b)), confirming presence of free silicon. The binding energy of SiC is reported[28,29] to be 100.3 eV. The peak of SiC was not observed at 100.3 eV in Si 2p spectrum, instead it was observed in the C 1s spectrum as a shoulder (binding energy 282.3 eV) to main C 1s peak (binding energy 284.2 eV[28]) (Fig. 3(c)). The 'difficulty' in bringing out the Si–C bonds appears inexplicable, though consistent, and should be noted for future reference. The C 1s peak at 284.2 eV also indicated presence of C–C bond.[28] In a word, the XPS spectrum confirmed presence of Si, SiC and carbon (free or in the form of graphite).

3.4. Microtexture

Results presented here were obtained under identical conditions of beam and camera set-up, and of acquisition and indexing. The microtextural characterizations using OIM had

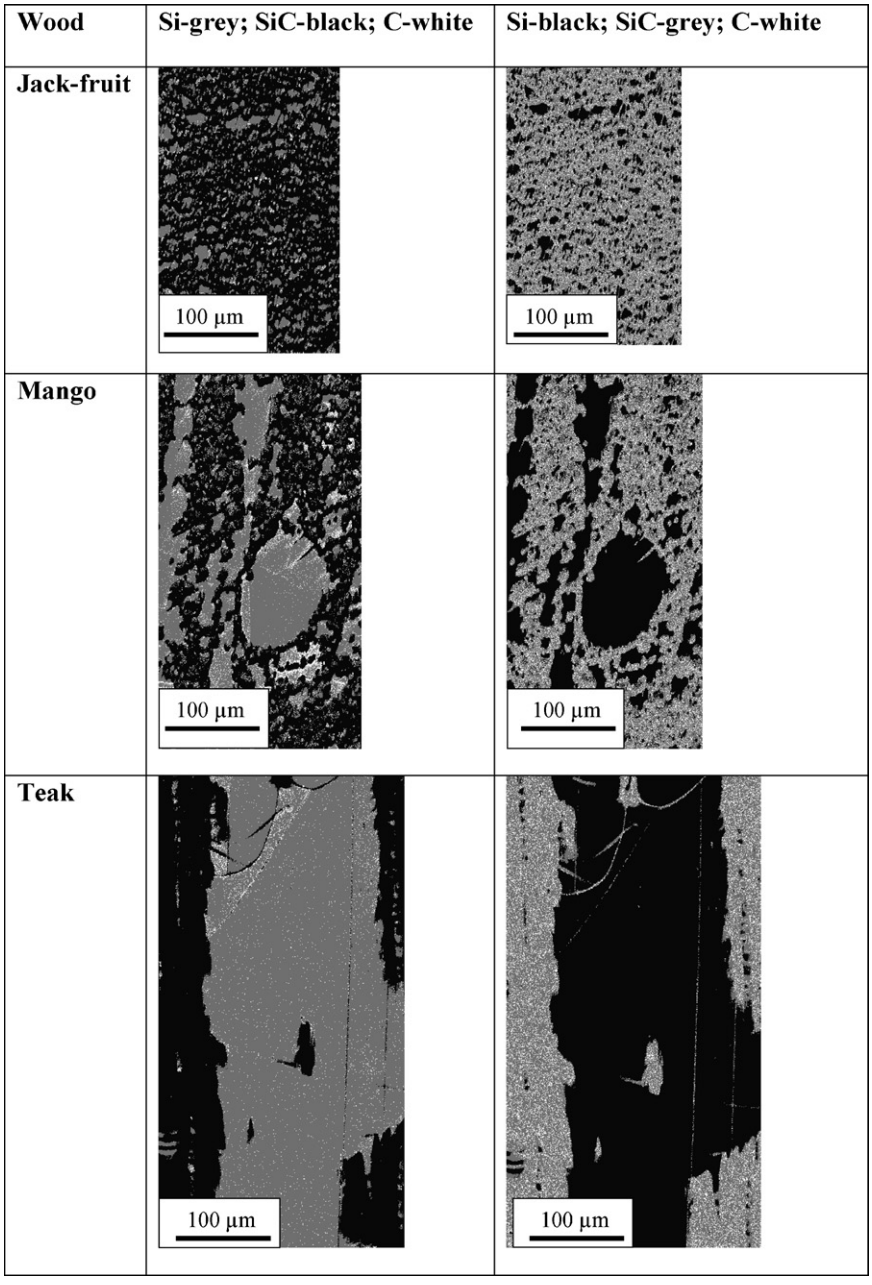

Fig. 4. Phase maps of the Si/SiC composites synthesized from three different wood.

Table 2
Phase proportion, average grain size and texture index (TI) of the constituent phases of cellular Si/SiC ceramic composites (which are estimated using OIM)

Ceramic composites	Phase proportion		Average grain size (μm)			TI	
	Si:C	SiC:C	Si	SiC	C	SiC	C
Si/SiC – jackfruit							
CI ≥ 0	0.21:0.03	0.56:0.18	23.0	0.9	1.4	144	402
CI > 0.03	0.3:0.01	0.16:0.05					
Si/SiC – mango							
CI ≥ 0	0.36:0.07	0.40:0.15	32.7	1.1	1.2	180	334
CI > 0.03	0.31:0.01	0.15:0.04					
Si/SiC – teak							
CI ≥ 0	0.56:0.02	0.31:0.10	51.0	2.7	2.1	203	340
CI > 0.03	0.48:0.005	0.13:0.02					

Notes: (1) Based on consistent differences in microhardness, microstructural features (as in Fig. 4) were distinguished primarily as regions containing SiC (protruded surface) and Si (plane surface). (2) TI was estimated following procedure described in Ref. [33]. (3) Confidence index (CI) in OIM is a measure of accurate indexing of Kikuchi pattern. The phase proportions of the Si, SiC and C is presented as scanned and for the data with confidence index, CI > 0.03.

one problem – cubic Si and β-SiC have identical crystal structures. These cannot be distinguished in a typical OIM scan. The polished specimens of the cellular Si/SiC ceramic composites showed two distinct topographical features – protruded surface and plane surface. The respective image qualities (IQ)[30] of the protruded (predominantly SiC) and plane (predominantly Si) surfaces however, provided an alternative.[b] SiC has lower atomic number (12.5 as compared to 14 for Si) and removal of distorted surface layer is also difficult in the hard SiC (see footnote). A combination of these two factors contributes to the low IQ values in SiC containing regions. Fig. 4 shows the phase map after partitioning of the OIM data using a criterion of IQ ≥ 20 (Si) and IQ < 20 (β-SiC). BSE image indicates presence of second phase inside the Si grains as is shown in Fig. 5(a). OIM scans provide more definite ID for this second phase – these were identified as graphite. Fig. 5(b) shows the captured image and the exact spot inside the Si grain from where the pattern was collected. Fig. 5(c) is the image of Kikuchi pattern from the said spot and Fig. 5(d) and (e) are the indexing using graphite and Si, respectively. It is evident from the indexed image that graphite gives better indexing of the observed bands than the Si as input phase. As shown in Fig. 5(b–e), graphite patterns could be indexed reliably and the existence of graphite, but not its exact content, was ascertained inside Si grains.

As shown in Fig. 4 and summarized in Table 2, the composites had typical microstructures of large Si grains surrounded by a network of fine SiC crystallites. Though graphite was also present inside the Si grains, most of the graphite did exist in the regions containing SiC. These observations were valid for all three composites, though there were also differences between the three performs – for example, the Si/SiC – jackfruit showed much finer distribution of Si than its counterparts synthesized from mango and teak woods .The large Si grains had a dominant presence of Σ3 (in coincident site lattice notation)[32] twin boundaries – 70–90% of the Si–Si boundaries fell into this class.

[b] The protruded region showed significantly higher hardness (2037 ± 200 HV) than the plane surface (969 ± 17 HV) – numbers close to the reported[31] values of SiC and Si, respectively.

The area fractions of Si, SiC and graphite are presented in Table 2, along with the respective grain sizes and texture index (TI)[33] values. Grain size of the different constituents was determined using a grain tolerance angle of 15°. The Si grains were found to be very coarse compared to SiC and graphite which showed comparable grain sizes. Texture index (TI) is a scalar quantity – it is defined as the integral of square of the ODF (orientation distribution function) intensity $f(g)$, $\mathrm{TI} = \int [f(g)]^2 \, \mathrm{d}g$, where g is an orientation.[33] TI for SiC and graphite in all the composites was obtained by first calculating texture using discrete binning approach. The parameters used for this method are: bin size of 5° and Gaussian smoothening of 5°. The number of grains covered for calculation of texture index (TI) of SiC and graphite respectively, were 8000 and 3700 (jack wood), 8000 and 2000 (mango wood) and, 5500 and 900 (teak wood). The numbers of grains/phases were considered large enough to provide quantitative estimates of relative texturing. TI values, as listed in Table 2, represent relative texturing or anisotropy. The graphite was clearly more textured than the SiC (see Table 2). Though no clear orientation relationships (ORs) could be established between Si–SiC or SiC–graphite, graphite and Si had clear and consistent OR. As shown in Fig. 6, in terms of axis-angle pairs two distinct ORs did emerge – 38 ± 1° ⟨4 3 2⟩ and 56 ± 1° ⟨22 17 7⟩. It is important to point out that these ORs were consistently applicable to Si–graphite of all three composites.

4. Discussion

A low temperature pyrolysis at 800 °C of common Indian dicotyledonous woods (mango, jackfruit and teak) followed by subsequent infiltration at 1600 °C of Si melt into the skeletal carbonaceous preforms could produce cellular Si/SiC ceramics with replication of cellular structural features of native woods in ceramic structures. A combination of XRD and XPS could establish the presence of cubic Si, cubic β-SiC and hexagonal graphite in all three types of cellular Si/SiC ceramic composites. The next real issue was to identify the exact location of these phases in the composite microstructures. Cubic Si and cubic β-SiC cannot be distinguished in an OIM scan. The hardness

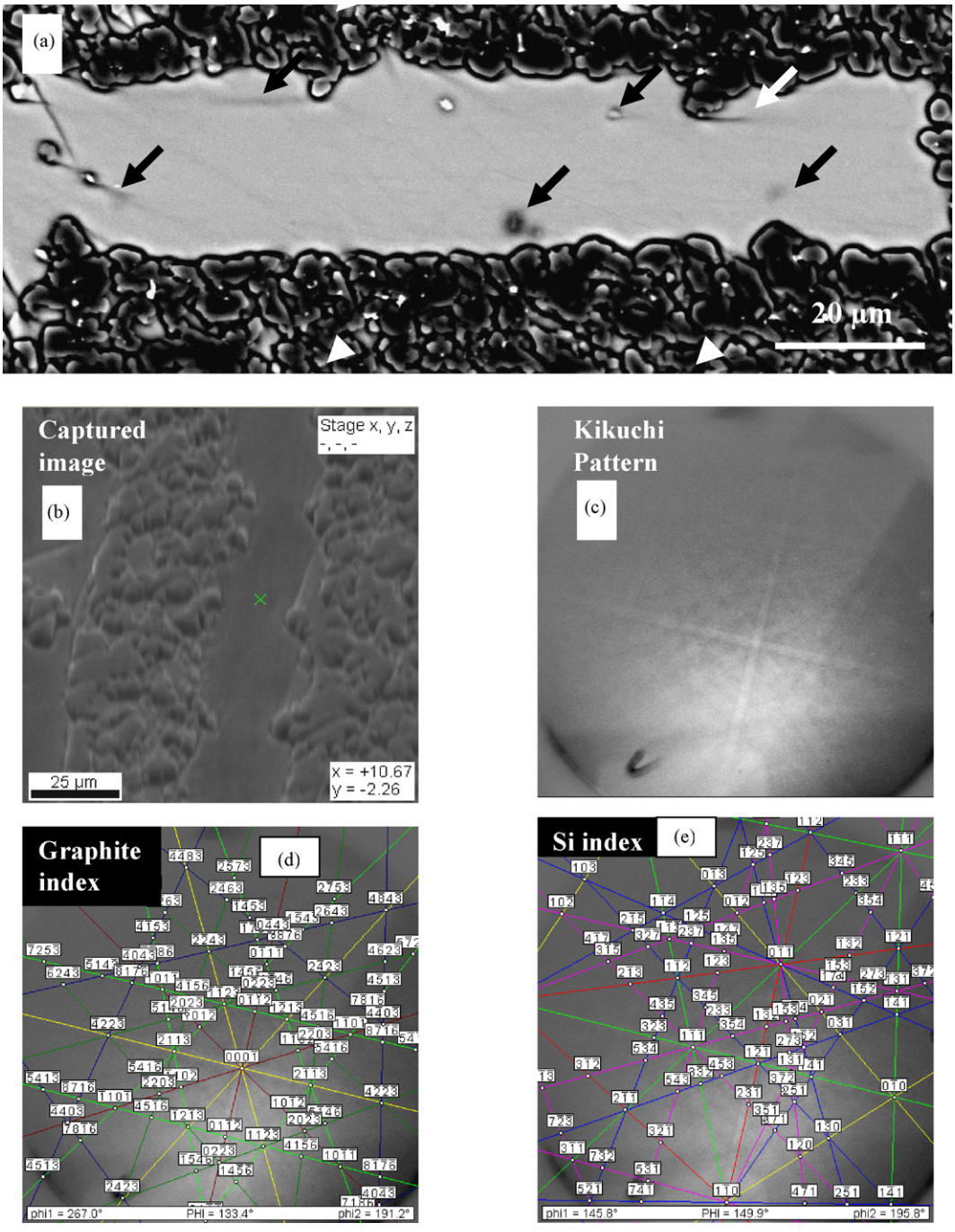

Fig. 5. (a) BSE image showing the location of graphite inside the Si grain, (b) captured image in OIM from where the kikuchi pattern for the graphite grain is collected, (c) kikuchi pattern for the said spot, (d) and (e) are the indexing using graphite and Si as the input phase. Based on confidence index and on visible pattern matching – presence of graphite inside Si grains could be established.

difference, however, was reflected on these two phases and they existed as protruded and plane surfaces – regions that could easily be distinguished in the OIM scans. This formulated the basis of the present study. It is to be noted that such studies have rarely been reported on wood derived SiC based composites – with one exception of an earlier, albeit limited, study.[9]

The experimental results obtained in the present investigation can be useful in understanding the process of microstructural evolution during synthesis of cellular Si/SiC ceramics. In fact liquid silicon infiltration (LSI) processing of SiC ceramics, including cellular Si/SiC ceramics, involves two conceptually independent processes of infiltration of liquid Si into channel pores present in the carbonaceous preforms and reaction between incoming Si and C which are not separable in practice at the LSI processing temperatures.[34,35] Capillarity is considered to be the main driving force for liquid infiltration[6,7,34,36] which is also valid in case of penetration of liquid Si into biocarbon preforms.[9,37] For the reaction mechanism, conflicting interpretations are available. Some authors reported continuous reaction product layers at the interface between C and Si that appeared

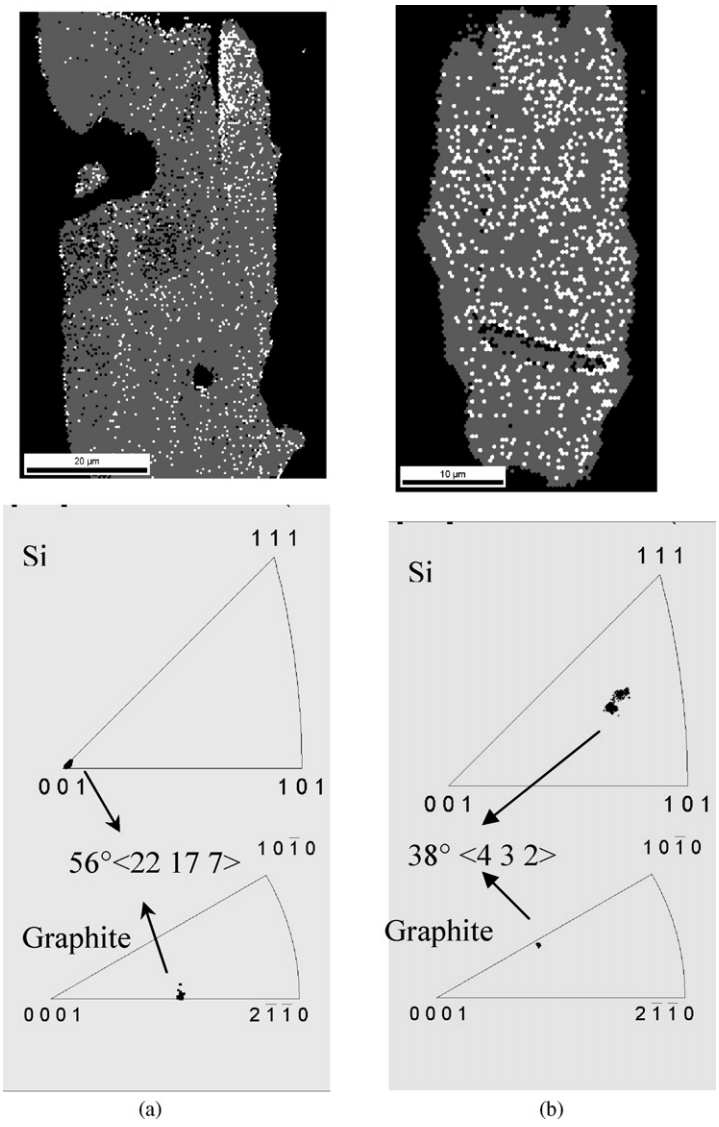

Fig. 6. OIM images of Si/SiC – mango showing large Si grains (grey) containing graphite (white) crystallites, with two distinct orientation relationships (ORs) emerging between the 'average' orientations of Si and graphite; such ORs are observed consistently in all three types of composites: (a) 56° ⟨22 17 7⟩ and (b) 38° ⟨4 3 2⟩.

to grow by a diffusion-controlled process; [34,35] no such continuous product layer was found by others[38–40] and it was suggested that the reaction product quickly spalled owing to volume misfit between SiC and C, leading to an interface-controlled reaction directly between Si and C. The other mechanism suggests repeating steps of dissolution of C in liquid Si followed by precipitation of SiC from supersaturated solution of C in Si, occur as the reaction front moves.[41–44] The solution-precipitation and interface-controlled mechanisms have similarity with regard to linear dependence of reaction rate on carbon solubility in Si, the C–Si reaction being assumed to be of first order with respect to C concentration.[40] For cellular Si/SiC ceramics, Greil et al.[9] attempted to explain the growth of the β-SiC layer into C struts with the help of diffusion-controlled mechanism, whereas interpretation of reaction of liquid Si and C of the pyrolyzed wood template in terms of solution-precipitation mechanism has become the theme of the work carried out by Zollfrank and Sieber.[37] The faceted morphology of the layer of reaction-formed SiC grains observed in the present study (Fig. 5(a)) indicates that they are grown from solution[40] and are consistent with the growth model via solution-precipitation, presented by Zollfrank and Sieber.[37] Absence of continuous reaction product layer observed during microscopic examination also provides support in favour of application of such a model in the present case. It, therefore, appears that during infiltration of liquid Si into porous carbon preform, simultaneous dissolution of carbon results in the formation of SiC in the carbon saturated Si-melt, as the carbon solubility in liquid Si is low at LSI temperature of the present study (around 3.5×10^{-2} at.% C in Si at 1600 °C[45]). It is likely that during initial stage of the reaction, a sub-micron sized layer of SiC is formed, which may act as the source and such stage continues until a sink of larger faceted grains of SiC develops.[37] The biocarbon preforms have fine distribution of porosity.[19] Because of this large surface area of the carbon in

biopreforms, the rate of dissolution of C in Si increases locally rising to levels of supersaturation[43] and providing the necessary driving force for the reaction to occur. It should be noted that the present experiment nearly parallels the LSI processing reported by Zollfrank and Sieber. For a LSI processing time of 40 min, as was adopted in the present investigation,[19] the model presented by Zollfrank and Sieber gives an average grain size of 4–5 μm for coarse-grained SiC, which closely tallies with those obtained in the present investigation (1–3 μm).

Though reports are available of the processing of cellular SiC based ceramics or composites from woods, involving graphitization of carbon during pyrolysis at high temperatures in the range of 1600–1800 °C for 4 h, prior to Si infiltration,[9,46] graphitization may also take place during the infiltration itself and the present study does agree with the general model presented by Zollfrank and Sieber[37] – though there is one contradiction. Clear presence of graphite inside the Si grains could be established both by backscattered imaging and by EBSD, the latter confirming presence of graphite. It is important to note that though the exact percentage of such graphite in the residual Si can be debated, its presence and the consistent orientation-relationship between Si and graphite appears conclusive. Silicon is a well known graphitizer in cast irons.[47] It may not be ruled out that fragments of SiC embedded in molten Si in channel pores undergo decomposition helping concurrent nucleation of both Si and graphite and evolving orientation relationship during solidification of Si. Such a model is far from complete, but appears reasonable as an approximation in explaining the presence of graphite inside the residual Si. The large Si grains had dominant presence of Σ3 twin boundaries – such boundaries are often reported[48] during solidification of liquid Si.

An earlier study on biomorphic Si/SiC ceramics involving pyrolysis of woods at 1800 °C for 4 h, has reported[9] $(1\,1\,0)_{SiC}//(0\,0\,0\,1)_{C}$ as possible orientation relationship (OR) between SiC and graphite. The present data, however, failed to bring out any clear ORs between SiC–graphite and Si–SiC. The graphite grains in the present study were clearly more textured than their host SiC – see the texture index (TI) values in Table 2.

5. Conclusions

(i) Liquid silicon infiltration processing (LSIP) of pyrolyzed Indian dicotyledonous woods (mango, jackfruit and teak) yielded cellular Si/SiC ceramic composites with structures that were replica of precursor plants.
(ii) Depending on the microcellular architecture of the initial wood, final ceramic composites exhibit a wide variation in microstructures.
(iii) X-ray diffraction (XRD) and X-ray photoelectron spectroscopy (XPS) established the presence of cubic Si, cubic β-SiC and hexagonal graphite in all three types of cellular Si/SiC ceramic composites.
(iv) The composites contained relatively large Si grains, presumably forming in the pores of the pyrolyzed woods, surrounded by fine grains of SiC. Most of the graphite was present in the SiC regions and this graphite was found to be more textured than the SiC.
(v) Finest distribution of Si filled pores was observed in jackfruit wood – area fraction of Si was highest in teak wood and lowest in jackfruit wood. In all cases Si grains had significant presence of Σ3 twin boundaries.
(vi) The graphite present in the large Si grains, however, showed clear orientation relationships – 56° ⟨22 17 7⟩ and 38° ⟨4 3 2⟩. These were valid consistently in all three cellular Si/SiC composites.

Acknowledgements

The authors wish to thank the Department of Science and Technology (DST), Government of India, for sponsoring the work (vide sanction no. SR/S3/ME/20/2003-SERC-Engg., dated 29.10.2004).They would like to acknowledge the use of DST (under IRPHA scheme) supported National Facility of Texture & OIM. The central facility for ESCA/Auger at IIT Bombay is also acknowledged.

References

1. Srinivasan, A. V., Haritos, G. K. and Hedberg, F. L., Biomimetics: advancing man-made materials through guidance of nature. *Appl. Mech. Rev.*, 1991, **44**(11), 463–482.
2. Vincent, J. F. V., Jeronimidis, G., Topping, B. H. V. and Khan, A. I., Biomimetics of flexible composites: towards the development of new materials. *Biomimetics*, 1992, **1**(4), 251–263.
3. Calvert, P., Biomimetic ceramics and composites. *Mater. Res. Soc. Bull.*, 1992, **17**(10), 37–40.
4. Heuer, A. H., Fink, D. J., Laraia, V. J., Arias, J. L., Calvert, P. D., Kendell, K. *et al.*, Innovative materials processing strategies: a biomimetic approach. *Science*, 1992, **255**, 1098.
5. Mark, J. E. and Calvert, P. D., Biomimetic, hybrid and in situ composites. *Mater. Sci. Eng.*, 1994, **C.1**, 175–186.
6. Popper, P., The preparation of self-bonded silicon carbide. In *Special Ceramics*, ed. P. Popper. British Ceramics Research Association, London, 1960, pp. 209–219.
7. Forrest, C. W., Kennedy, P. and Shennan, J. V., The Fabrication and properties of self-bonded silicon carbide. In *Special Ceramics*, *vol. 5*, ed. P. Popper. British Ceramic Research Assocation, London, 1972, pp. 99–123.
8. Ota, T., Takahashi, M., Hibi, T., Ozawa, M., Suzuki, S., Hikichi, Y. *et al.*, Biomimetic process for producing SiC wood. *J. Am. Ceram. Soc.*, 1995, **78**(12), 3409–3411.
9. Greil, P., Lifka, T. and Kaindl, A., Biomorphic cellular silicon carbide ceramics from wood. *J. Eur. Ceram. Soc.*, 1998, **18**(14), 1961–1973.
10. Singh, M., Environment conscious ceramics. *Ceram. Eng. Sci. Proc.*, 2000, **21**(4), 39–44.
11. Shin, D. W., Park, S. S., Choa, Y. H. and Niihara, K., Si/SiC composites fabricated by infiltration of a Si melt into charcoal. *J. Am. Ceram. Soc.*, 1999, **82**(11), 3251–3253.
12. Vogli, E., Mukerji, J., Hoffman, C., Kladny, R., Sieber, H. and Greil, P., Conversion of oak to cellular silicon carbide by gas-phase reaction with silicon monoxide. *J. Am. Ceram. Soc.*, 2000, **84**(6), 1236–1240.
13. Vogli, E., Sieber, H. and Greil, P., Biomorphic SiC-ceramic prepared by Si-gas phase infiltration of wood. *J. Eur. Ceram. Soc.*, 2002, **22**(14-15), 2663–2668.
14. Sieber, H., Friedrich, H., Schwarze, D., Kaindl, A. and Greil, P., Ceramic light weight structures from paper derived composites. In ed. J. P. Singh, N. P. Bansal and K. Niihara. In *Ceramic Transactions*, *vol. 108*. The American Ceramic Society, Ohio, 2000, pp. 571–580.
15. Byrne, C. E. and Nagle, D. E., Cellulose derived composites – a new method for materials processing. *Mater. Res. Innovat.*, 1997, **1**, 137–145.
16. Chakrabarti, O. P., Maiti, H. S. and Majumdar, R. Indian patent, 0481 NF 2002/IN, Council of Scientific and Industrial Research, India, 2004.

17. Chakrabarti, O. P., Maiti, H. S. and Majumdar, R. Indian patent, 0480 NF/2002/IN, Council of Scientific and Industrial Research, India, 2004.
18. Chakrabarti, O. P., Maiti, H. S. and Majumdar, R., Si/SiC ceramics from plant precursor. *J. Mater. Sci.*, 2004, **39**(14), 4715–4717.
19. Chakrabarti, O. P., Mallick, D., Maiti, H. S. and Majumdar, R., Microcellular Si/SiC ceramics by replication of indian dicotyledonous woods. *Trans. Ind. Ceram. Soc.*, 2006, **65**(1), 23–28.
20. Mallick, D., Chakrabarti, O. P., Maiti, H. S. and Majumdar, R., Si/SiC ceramics from biostructures of some Indian dicotyledonous and monocotyledonous plants. *Ceram. Int.*, in press.
21. Singh, M. and Salem, J. A., Mechanical properties and microstructure of biomorphic silicon carbide ceramics fabricated from wood precursors. *J. Eur. Ceram. Soc.*, 2002, **22**(14–16), 2709–2717.
22. Qiao, G., Ma, R., Cai, N., Zhang, C. and Jin, Z., Mechanical properties and microstructure of Si/SiC materials derived from native wood. *Mater. Sci. Eng.*, 2002, **A 323**, 301–305.
23. Singh, M., Fernandez, J. M. and de Arellano-Lopez, A. R., Environmentally conscious ceramics (Ecoceramics) from natural wood precursors. *Curr. Opin. Solid-State Mater. Sci.*, 2003, **7**, 247–254.
24. Zollfrank, C. and Sieber, H., Microstructure and phase morphology of wood derived biomorphous SiSiC-ceramics. *J. Eur. Ceram. Soc.*, 2004, **24**(2), 495–506.
25. Schulte-Fischedick, J., Zern, A., Mayer, J., Rühle, M., Frieβ, M., Krenkel, W. *et al.*, The morphology of silicon carbide in C/C–SiC composites. *Mater. Sci. Eng.*, 2002, **A332**, 146–152.
26. Randle, V., *Microtexture Determination and its Applications*. The Institute of Materials, London, 1992.
27. Chakrabarti, O. P., Weisensel, L. and Sieber, H., Reactive melt infiltration processing of biomorphic Si–Mo–C ceramics from wood. *J. Am. Ceram. Soc.*, 2005, **82**(7), 792–798.
28. Iwanowski, R. J., Fronc, K., Paskowicz, W. and Heinonen, M., XPS and XRD study of crystalline 3C–SiC grown by sublimation method. *J. Alloys Compd.*, 1999, **286**, 143–147.
29. Pivac, B., Furic, K., Milun, M., Valla, T., Borghesi, A. and Sassella, A., Spectroscopic study of SiC-like structures formed on polycrystalline silicon sheets during growth. *J. Appl. Phys.*, 1994, **75**, 3586–3592.
30. Mott, B. W., *Micro-Indentation Hardness and Testing*. Butterworths Scientific Publications, London, 1956.
31. *OIM – 4.0, User Manual*, ed. TSL-EDX, TexSEM Laboratories, USA, 2004.
32. Randle, V. and Engler, O., *Introduction to Texture Analysis: Macrotexture Microtexture and Orientation Mapping*. Gordon and Breach, London, 2000.
33. Yerra, S. K., Verlinden, B. and Van Houtte, P., On crystallographic texture of as-drawn doped-W wires. *Mater. Sci. Forum*, 2005, **495–497**, 913–918.
34. Fitzer, E. and Gadow, R., Fibre reinforced silicon carbide. *Am. Ceram. Soc. Bull.*, 1986, **65**(2), 326–335.
35. Zhou, H. and Singh, R. N., Kinetics model for the growth of silicon carbide by the reaction of liquid silicon with carbon. *J. Am. Ceram. Soc*, 1995, **78**(9), 2456–2462.
36. Hillig, W. B., Mehan, R. L., Morelock, C. R., De Carlo, V. J. and Laskow, L., Silicon/silicon carbide composite. *Am. Ceram. Soc. Bull.*, 1975, **54**(12), 1054–1056.
37. Zollfrank, C. and Sieber, H., Microstructure evolution and reaction mechanism of biomorphous SiSiC ceramics. *J. Am. Ceram. Soc.*, 2005, **88**(1), 51–58.
38. Minnear, W. P., Interfacial energies in Si/SiC system and the Si + C reaction. *J. Am. Ceram. Soc.*, 1982, **65**(1), C10–C11.
39. Hase, T., Suzuki, H. and Iseki, T., Rise in temperature of SiC pellet involving reaction sintering. *J. Nucl. Mater.*, 1976, **59**(1), 42–48.
40. Chiang, Y. M., Messner, R. P. and Terwilliger, C. D., Reaction formed silicon carbide. *Mater. Sci. Eng.*, 1991, **A114**, 63–74.
41. Pyzalski, M., Bialoskorski, J. and Walasek, E., Reaction between carbon fibres and molten silicon: heat determination using DTA. *J. Therm. Anal.*, 1986, **31**, 1193–1196.
42. Pampuch, R., Walasek, E. and Bialoskorski, J., Mechanism of reactions in $Si_l + C_f$ system. *Ceram. Int.*, 1987, **13**(1), 63–68.
43. Sawyer, G. R. and Page, T. F., Microstructural characterization of REFEL (reaction bonded) silicon carbide. *J. Mater. Sci.*, 1978, **13**(4), 885–904.
44. Chakrabarti, O. P., Das, P. K. and Mukerji, J., Growth of SiC particles in reaction sintered SiC. *Mater. Chem. Phys.*, 2001, **67**, 199–202.
45. Scace, R. T. and Slack, S. A., Solubility of carbon in silicon and germanium. *J. Chem. Phys.*, 1959, **30**(6), 1551–1555.
46. Herzog, A., Klingner, R., Vogt, U. and Graule, T., Wood derived porous SiC ceramics by sol infiltration and carbothermal reduction. *J. Am. Ceram. Soc.*, 2004, **87**(5), 784–793.
47. Smith, S. W., *Foundations of Materials Science and Engineering* (*3rd ed.*). McGraw Hill, International edition, 2004, p. 495.
48. Heiberg, G. and Arnberg, L., Investigation of the microstructure of the Al–Si eutectic in binary aluminium–7 wt.% silicon alloys by electron backscatter diffraction (EBSD). *J. Light Met.*, 2001, **1**, 43–49.